PHYSICAL REVIEW B

CONDENSED MATTER

THIRD SERIES, VOLUME 45, NUMBER 23 15 JUNE 1992-I

Photoinduced defects in the bromide-bridged platinum linear chain $[Pt(en)_2][Pt(en)_2Br_2](ClO_4)_4$ (with en=ethylenediamine)

Robert J. Donohoe,* Laura A. Worl, C. Anthony Arrington,† Alain Bulou,‡ and Basil I. Swanson*

Inorganic and Structural Chemistry Group, INC-4, MS-C345, Los Alamos National Laboratory, Los Alamos, New Mexico 87545

(Received 28 October 1991; revised manuscript received 14 February 1992)

Photoinduced defects in the bromide-bridged platinum linear chain $[Pt(en)_2][Pt(en)_2Br_2](ClO_4)_4$ (PtBr, where en=ethylenediamine) yield Raman, absorption, and electron paramagnetic resonance (EPR) signals that have been examined as a function of temperature in order to determine the kinetics of the decay of these metastable defects in an intermediate-strength low-dimensional charge-density-wave (CDW) solid. Both diamagnetic and paramagnetic defects are photogenerated with the initial excitonic transient primarily decaying to form electron bipolarons and hole polarons. The photogenerated Raman signal is indicative of the former and the EPR signal of the latter. The type and stability of these photoinduced defects are dependent on the sample history, with PtBr crystals grown in the orthorhombic phase (above 30 °C) leading to greater variety and stability of defects as compared with those photoinduced in crystals grown in the monoclinic phase (below 10 °C). The temperature dependence of the photogenerated spectroscopic signals reveals complicated decay routes, with the eventual recombination of valence defects mediated by lattice pinning potentials of various strengths, interconversion of defect states (including the possible "melting" of electron bipolarons into electron polarons) and a strengthening of the CDW as the crystals are warmed toward room temperature. The observation of bromide hyperfine splitting in the EPR data and the reversible intensity changes in the Raman defect signals indicates that these defects are spatially quite disperse, with ten or greater platinum sites revealed in the EPR signal, and demonstrates that the weakening of the CDW in PtBr relative to the strong CDW solid PtCl has a significant effect on the ground- and defect-state properties.

INTRODUCTION

The halide-bridged mixed-valence metal linear chains (*MX*) have played a prominent role in the development of theoretical and experimental techniques for the examination of highly correlated narrow-band electronic materials.[1–8] Much of the utility of these materials lies in their crystalline quasi-one-dimensional structure, which greatly simplifies experimental characterization and theoretical modeling, thereby allowing detailed exploration of the electron-electron and electron-phonon forces that determine electrical and optical properties. Practical applications for *MX* chains, such as incorporation into nonlinear optical devices and as chemical sensors, have also been suggested and are currently being explored. Most *MX* chains exhibit spectroscopic and crystallographic properties characteristic of Peierls-distorted strongly correlated charge-density-wave (CDW) materials. The strength of the CDW is manifested by the extent to which the halide sublattice is dimerized and the corresponding charge disproportionation of the metal sublattice, which affects the energy of the characteristic intervalence charge-transfer (IVCT) absorption exhibited by these materials. Two recent reports emphasize the tunability of the electronic structures in *MX* chains. Toriumi *et al.* have reported a non-Peierls-distorted chain comprised of NiBr units.[9] On the basis of susceptibility data, the ground state in this solid was assigned to a spin-density wave (SDW). However, recent theoretical calculations that employ a two-band Peierls-Hubbard model suggest that a spin-Peierls structure in which the Ni sublattice is slightly dimerized should be the preferred ground-state structure.[10] A very interesting paper by Haruki and Wachter indicates a magnetic ordering phase transition in the weak CDW *MX* chain PtI under strong magnetic fields.[11]

The *MX* chain $[Pt(en)_2][Pt(en)_2Br_2](ClO_4)_4$ (en=ethylenediamine), referred to hereafter as PtBr, exhibits an intermediate-strength CDW phase when compared with the chloride analogue, PtCl, which is a strong CDW material, and with PtI, which exhibits only slight halide sublattice distortion. Much of the previous literature on PtBr has been brought into question by the

discovery of Huckett *et al.* that the traditional synthetic route to PtBr results in incorporation of approximately 11% chloride (by NMR) at the bridging position.[2(b)] Because the contamination of PtBr by chloride has been pervasive in our materials until a new synthetic strategy was adopted, we expect that other workers have, in general, examined impure materials. However, the elemental analyses that have been reported are excellent and the levels of chloride in samples examined in other laboratories may have been reduced by multiple recrystallizations or some other means. In any case, several puzzling reports on PtBr appear to be explained by the presence of chloride doping. As an example, the resonance Raman (RR) data for PtBr are heavily dependent upon the extent of chloride doping. The RR spectra collected in resonance with the intervalence charge-transfer band (IVCT, low-energy edge near 1.5 eV, *vide infra)* for pure PtBr exhibit only the fundamental and overtones of the zone-center optic mode (ν_1, 166 cm^{-1}), while the doped samples yield additional features. These include both the vibrational peak expected for the chloride domains as well as peaks that are unobserved in either of the pure materials but gain intensity in the mixed-halide solids due to perturbation of the electronic structure at the juncture of differing halide domains (edge states). Structural studies of PtBr have also been affected by chloride doping, not only due to variation in the position of the bridging halide but also because the pure materials undergo a monoclinic to orthorhombic phase transition that occurs above room temperature for pure PtBr (30 °C) and below room temperature for pure PtCl (19 °C). In the mixed-halide chains, the phase change remains sharp but the onset temperature appears to vary smoothly as a function of composition. Therefore, chloride doping can result in orthorhombic PtBr at ambient conditions.[8(f)]

With the proper synthetic route established, we have undertaken a spectroscopic examination in order to characterize both the ground- and photoinduced-defect-state properties of pure PtBr. The present study is motivated in part by the opportunity to compare PtBr with PtCl, which has already been extensively examined. In this regard, the two-band model of the *MX* materials as developed by Bishop *et al.* suggests that the relative weakening of the CDW in PtBr as compared to PtCl will affect the nature of defect states in several distinct ways, including greater delocalization of defects in PtBr, changes in the energies of the subgap defect electronic absorptions relative to the IVCT edge, and a possible increase in the variety of defect states observed above the IVCT absorption (ultragap states).[3(i),10]

Our studies include examination of the effects of photolysis on the absorption, Raman, and EPR spectroscopic response in PtBr. We have monitored the relaxation of the photoinduced defects as a function of temperature and have observed complicated kinetics that are affected by interconversion of defect states, the presence of pinning sites of varying strengths, and a change in the strength of the ground-state CDW. We have also observed a strong dependence of the spectroscopic signals and defect kinetics on the phase in which the crystals were grown (monoclinic phase below and orthorhombic phase above 29.8 °C) despite the fact that, by calorimetry, the phase change appears to be reversible[2(b)] and the spectroscopic measurements for both types of materials were undertaken at identical temperatures. The classical lattice-dynamics calculations we have performed for PtCl [Ref. 12(a)] have now been extended to include defect and normal chain modes for PtBr, and some of the results from these calculations are included herein as an aid to assignment of defect modes. An alternative to the classical dynamics studies of defect phonons has been developed, and we briefly address these new descriptions of the defect phonons.

EXPERIMENT

The PtBr solid was synthesized by method *C* of Ref. 2(b). In order to minimize the photoinduced defects prior to spectroscopic examination, the PtBr samples were crystallized in the dark and loaded on sample cells under reduced-light conditions. The crystals used in this study were selected from batches grown in both the monoclinic and orthorhombic phases (crystallized at 5 °C and 40 °C, respectively) that yielded no detectable chloride contamination by either NMR or RR measurements. Both the red and near-infrared and the visible excitation resonance Raman instruments have been described elsewhere.[5(h),5(i)] All of the red and near-infrared RR measurements were made with 2 mW or less excitation power, and the visible excitation RR data were collected with less than 5-mW power. Except where noted, the RR data were acquired at a nominal temperature of 13±2 K.

Single-crystal absorption measurements were performed on crystals of approximately 100-μm thickness. Such a thickness precludes measurable transmission in the IVCT region, and we use the absorption measurement solely for the purpose of examination of the subgap defect states. The crystals were mounted (at a 45° angle to minimize the polarization dependence of the instrument response) over a 300-μm aperature drilled in a copper disc that was coupled to a displex cryostat. The mounted crystals were examined under cross polarizers to check for light leaks around or through the crystal. It should be noted that exclusion of light prior to making a subgap absorption measurement is not possible and some photolysis probably occurs during mounting, when the crystals are examined under the microscope, and during alignment in the spectrometer sample chamber. The data were collected in the single-beam mode with a prism polarizer after the sample in order to examine the polarization of the defect transition dipoles. Photolysis of the crystals was accomplished by use of the spectrometer source lamp with the monochromator set to 2.41 eV.

The EPR data were collected with an IBM Instruments model ER-200 *X*-band EPR spectrometer typically with 20-mW power and 20-G modulation amplitude. Crystals were oriented perpendicular to the magnetic field. For the EPR experiments, the samples were cooled by a temperature-controlled liquid-helium transfer cryostat. The photoinduced EPR signal was generated with both visible radiation from an argon-ion laser (all lines) and with irradiation from a mercury lamp.

RESULTS AND DISCUSSION

Absorption data

Because of the crystal morphology, acquisition of quality single-crystal low-temperature polarized absorption data is much more difficult for PtBr than for PtCl. We have concluded that the absorption edge for the IVCT transition in PtBr occurs near 1.5 eV, in contrast to earlier reports that place it near 1.2 eV.[4(j)] This conclusion is not only based upon the absorption results, which are very noisy in this region, but also upon the resonance Raman data, which reveal an increase in the intensities of the overtones of the ν_1 mode relative to the fundamental as excitation is tuned above 1.5 eV and into resonance with the IVCT. Very close correspondence of the overtone-fundamental intensity ratio from the Raman data and the IVCT absorption profile is observed in PtCl.[5(i)]

The occurrence of a phase change at 29.8 °C in undoped PtBr led us to investigate the effects of crystallization above and below this transition on the spectroscopy of PtBr. The near-infrared electronic absorption data as a function of photolysis at 20 K for pure PtBr crystallized at 40 °C (in the orthorhombic form) are displayed in Fig. 1. The corresponding data for PtBr crystallized in the monoclinic form are similar. For the purpose of brevity, we hereafter refer to these two types of samples as PtBr(O) and PtBr(M), respectively. Photolysis of both PtBr(O) and PtBr(M) results in increased intensity for at least one defect absorption band at 1.2 eV. (This band may be the cause of the earlier report of the IVCT edge in this region.) Upon warming to room temperature and recooling, the intensity for the photoinduced band in samples of PtBr(M) is largely obliterated while some of that for PtBr(O) samples remains. Assignment of the photoinduced absorption band is greatly aided by analysis of the resonance Raman results, and we defer description of this transition until the vibrational data have been presented.

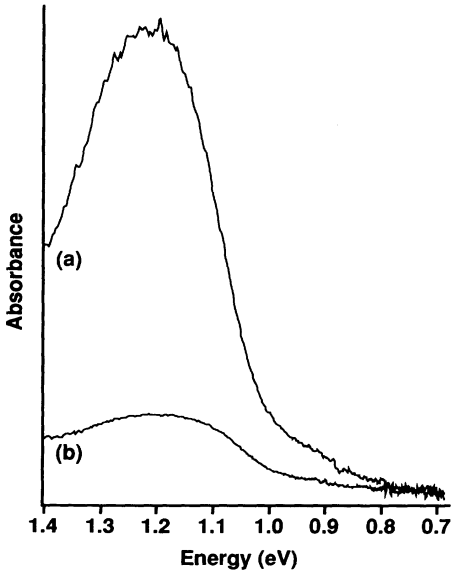

FIG. 1. The near-infrared absorption of a single crystal of PtBr(O) at 20 K (a) after and (b) before photolysis with 2.41-eV excitation. The absorption is polarized parallel to the PtBr chain axis.

Resonance Raman data

Subgap excitation

The RR spectra acquired with 1.26-eV excitation as a function of photolysis for a single crystal of the PtBr(M) material are shown in Fig. 2. Prior to photolysis, the observable peaks include the intense ν_1 band (166 cm^{-1}, off scale), a weak peak at 95 cm^{-1}, which may be the chain-polarized infrared-active mode reported by DeGiorgi *et al.* at 110 [Ref. 6a)] or 95 [Ref. 6(b)] cm^{-1}, and a weak shoulder at approximately 180 cm^{-1}. In the RR data, the 95-cm^{-1} peak appears to track the intensity of the ν_1 peak but can be used as a rough intensity standard for the photoinduced defect modes. Upon photolysis, a dramatic increase in intensity is observed for a broad, asymmetric, chain-axis-polarized peak at 130 cm^{-1}. A weak peak near 90 cm^{-1} also appears. These photoinduced RR peaks were observed to reach roughly constant intensity after 1 h of photolysis with the all-lines output of an Ar^+ laser at a power density of 2 mW/mm^2. The excitation dependence for the red-near-infrared region of *photolyzed* PtBr(M) is shown in Fig. 3. In this figure, the intensity of the ν_1 peaks (counts at the maximum less the baseline

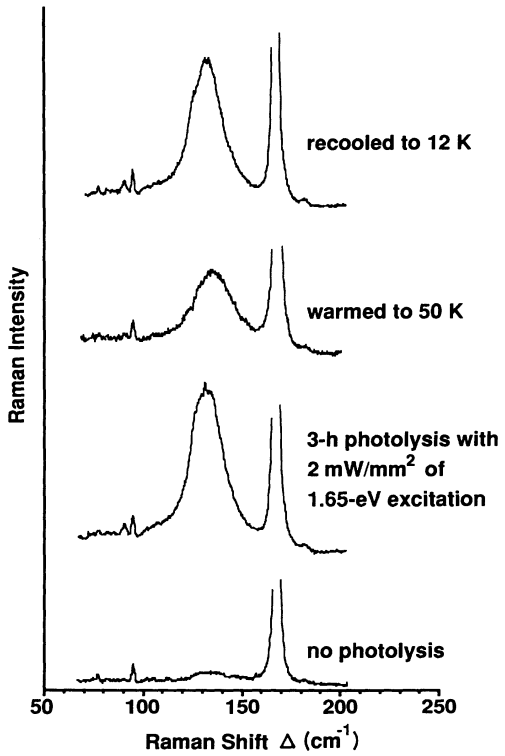

FIG. 2. The Raman spectrum of PtBr(M) with 1.26-eV excitation as a function of photolysis and then temperature. The intense ν_1 peak at 166 cm^{-1} is off scale to facilitate viewing of the 130-cm^{-1} feature, which attains roughly 10% peak intensity relative to the ν_1 mode after photolysis.

counts) was set to a single value for all of the spectra prior to expansion by a constant factor. As is seen in the figure, the intensity of the 130-cm^{-1} feature relative to the ν_1 and 95-cm^{-1} modes increases as the excitation is tuned toward the red extreme of our instrument sensitivity. In addition, an overtone for this peak, at 260 cm^{-1} (not shown), is observed to increase its intensity *relative* to the 130-cm^{-1} fundamental as the excitation energy is tuned to the red. These observations indicate that the 130-cm^{-1} peak is vibronically associated with the photoinduced defect absorption shown in Fig. 1. No other photoinduced RR peaks were observed with excitations between 1.50 and 1.26 eV.

The RR spectra for an *unphotolyzed* sample of PtBr(O) as a function of excitation energy in the red and near infrared are displayed in Fig. 4. As before, the ν_1 mode is set to a constant intensity prior to expansion. Several marked differences occur between the RR data of this sample and the PtBr(M) sample. The 130-cm^{-1} peak is observed prior to photolysis even though the crystal has been incubated at room temperature in the dark for several days prior to data acquisition. This suggests that the defect associated with the 130-cm^{-1} peak is stabilized to some extent in PtBr(O) even at room temperature. Even more striking is the observation that the PtBr(O) samples exhibit a set of excitation-dependent peaks between 150 and 160 cm^{-1} that are unobserved in the samples crystallized in the monoclinic form. An unresolved peak at approximately 160 cm^{-1} is observed upon irradiation with 1.46-eV excitation energy while a peak at 155 cm^{-1} is enhanced with 1.34-eV excitation and a sharp feature at 150 cm^{-1} is enhanced with 1.26-eV excitation.

As is the case for PtBr(M), the intensity of the 130-cm^{-1} peak in samples of PtBr(O) is dramatically increased by photolysis (not shown). However, at 12 K, the 160–150-cm^{-1} peaks do not appear to gain intensity as a direct result of photolysis.

The metastability of photoinduced defects in the strong CDW solid PtCl is such that several hours at room temperature are required to diminish the observed defect absorptions to their prephotolysis levels.[4(e),4(g)] For PtBr(M), this is also the case, as determined by warming the samples to room temperature overnight, followed by recooling and examination of the RR spectra. However, for PtBr(O), the photoinduced signals are only partially removed by incubation at room temperature even when the sample is rigorously maintained under darkened conditions for several days. Thus, the defects responsible for the 130-cm^{-1} phonon are stabilized to a greater extent in samples of PtBr(O). This is similar to the behavior seen in the EPR data *(vide infra)*, where the paramagnetic defects appear to be stabilized in both PtBr(M) and PtBr(O) by external pinning forces that adopt a variety of magnitudes, with stronger pinning observed in the samples of PtBr(O).

In an effort to monitor the decay of the photoinduced defects, we examined the absorption and RR spectra of the photolyzed samples as a function of temperature. Upon warming the photolyzed samples of PtBr(M) to 50 K (Fig. 2), we observed extensive decay of the 130-cm^{-1} RR signal intensity. The maximum of this peak also shifts slightly to greater Raman shift. Interestingly, this

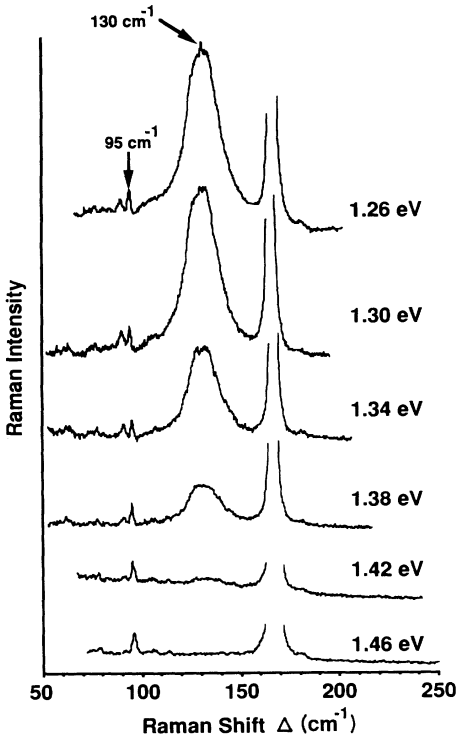

FIG. 3. The near-infrared excitation dependence of the Raman spectrum of a photolyzed sample of PtBr(M).

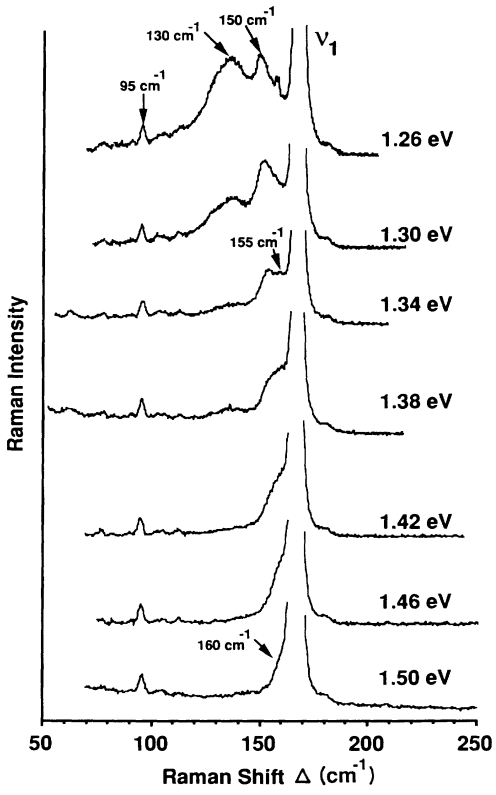

FIG. 4. The near-infrared excitation dependence of the Raman spectrum of a unphotolyzed sample of PtBr(O).

loss of intensity, clearly not a result of Boltzmann effects (compare the intensity relative to the 95-cm^{-1} peak), can be almost completely reversed by recooling the sample, as shown in Fig. 2. We interpret this as an indication of mobilization or interconversion of defects in PtBr. In the first instance, we could lose intensity of the defect phonon due to alteration of its spatial and electronic properties as it is mobilized. In the second scenario, conversion of the 130-cm^{-1} defect into a different type of defect that is not in resonance with the Raman probe energy could explain the loss of signal. In any case, the recovery of the 130-cm^{-1} intensity upon recooling is a remarkable point that indicates that the 130-cm^{-1} defects are not being rapidly converted into normal chain sites by mobilization and recombination of valence defects. If such were the case, we would not expect that the defect phonon intensity could be recovered by simple recooling of the sample. As will now be discussed, direct evidence for interconversion of defects in PtBr is observed in photolyzed samples of PtBr(O).

As shown in Fig. 5, the 130-cm^{-1} RR peak is also diminished by raising the temperature of photolyzed samples of PtBr(O). At the same time, the intensity of the 150-cm^{-1} peak is increased. This strongly suggests the temperature-induced interconversion of defects in samples of PtBr(O). The 150-cm^{-1} peak does not appear to be reconverted into the 130-cm^{-1} peak upon recooling. As can be seen in Fig. 6, after several cooling-photolysis-rewarming cycles, the relative intensity of the 150-cm^{-1} peak is permanently increased. Therefore, there are distinct defect sites that yield 130- and 150-cm^{-1} phonons (although the possibility remains that some of the intensity of the 130-cm^{-1} peak may be associated with the 150-cm^{-1} peak). Furthermore, the apparent interconversion of the 130- and 150-cm^{-1} defects does not appear to be the result of a thermally controlled equilibrium, but rather entails the generation of one type of defect that is mobilized and converted into a new form of defect due to a trap that is unique to the PtBr(O) material.

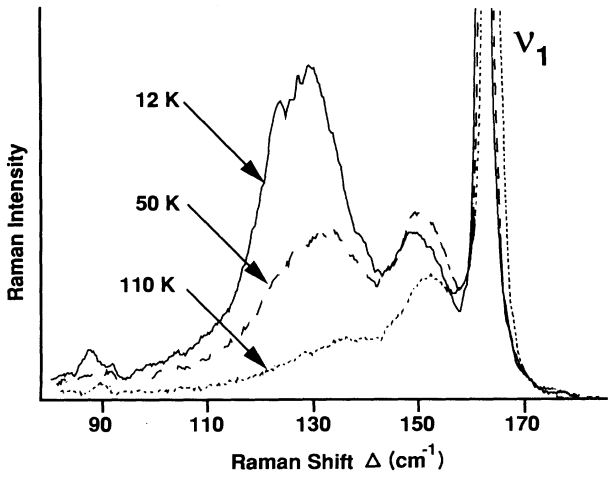

FIG. 5. The temperature dependence of the 1.26-eV excitation Raman spectrum of a photolyzed sample of PtBr(O). Note the shift in the ν_1 peak energy (see text).

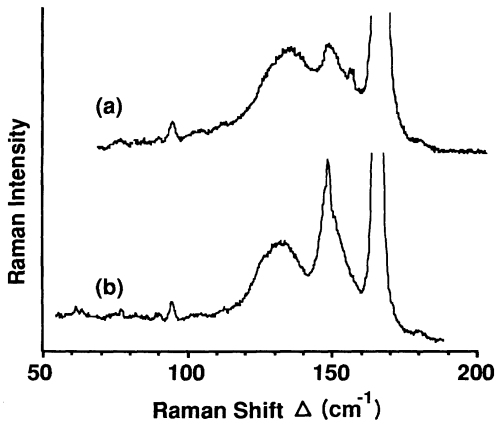

FIG. 6. Comparison of the 1.26-eV excitation Raman spectra of a PtBr(O) crystal (a) before photolysis and (b), after several photolysis and warming cycles.

The temperature dependence of the Raman defect data should be compared with that of the photoinduced absorption (not shown). Upon warming, the photoinduced absorptions observed in our data for both types of samples broaden, shift slightly to the blue, and lose intensity. This blueshift upon warming is also observed in the absorption edge reported by Matsushita *et al.*,[4(j)] which we attribute to the 1.2-eV defect transition. Although this shift may be due to defect interconversion, the effect is not remarkable enough to be definitive. Furthermore, there is no conclusive indication of recovery of photoinduced defect absorption after warming and recooling.

Ultragap excitation

Resonance Raman data have also been obtained with excitation energies above the IVCT edge. Interpretation of the results from this experiment is complicated by the fact that the probe beam photolyzes the crystals. The RR data for a sample of PtBr(M) at 13 K as a function of tuning the excitation above the IVCT edge are shown in Fig. 7. These data are remarkable on several accounts. First, there are new features at 182 and 174 cm^{-1} that are not due to dispersion of the ν_1 peak at 166 cm^{-1}. An additional unresolved feature at approximately 171 cm^{-1} is also present, as determined by curve analysis and by observation of an overtone at 340 cm^{-1}. These RR peaks demonstrate the presence of defect transitions above the IVCT absorption. Such a conclusion is substantiated by examination of the overtone region. For example, the 174-cm^{-1} peak is not the most intense feature in the fundamental region upon excitation with 2.41 eV, but the overtone at 347 cm^{-1} is the dominant peak in that portion of the RR spectrum. This demonstrates that the resonance enhancement of the 174-cm^{-1} mode is greater in this region and indicates the presence of a distinct absorption. The presence of transitions above the IVCT (excluding the ultraviolet ligand-based absorptions), which we term ultragap states, is not expected within models that neglect the filled halide band, but is predicted by the three-fourths-filled two-band model.[3(i),5(j)] Thus, these defect states may arise due to transitions from the

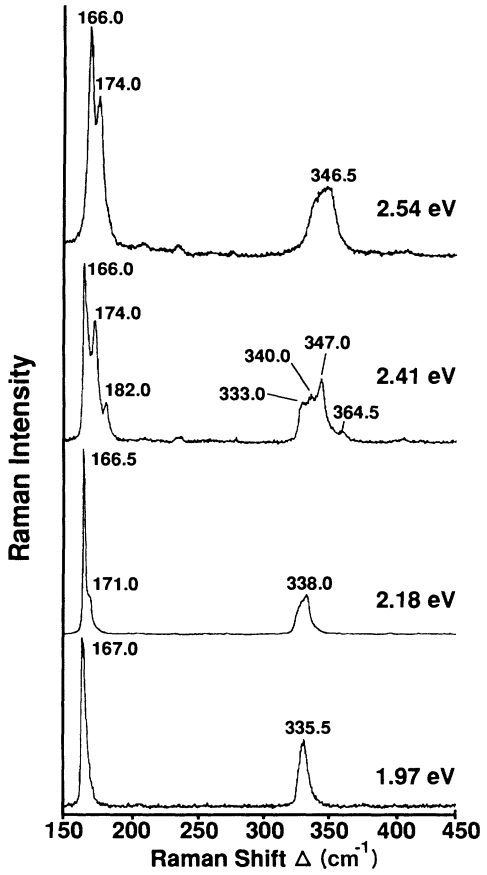

FIG. 7. The excitation dependence of the Raman spectrum of a sample of PtBr(M) obtained with excitation energies above the IVCT absorption edge.

halide bands to midgap levels in the metal band. In particular, hole bipolarons are expected to yield such absorptions. In intermediate to weak CDW systems, ultragap states are also expected for hole polarons.[3(i)] In this regard, examination of Fig. 7 reveals that the two peaks at 182 and 174 cm^{-1} change their relative intensities both with respect to each other and as compared with the normal chain 166-cm^{-1} peak. This shows that these peaks are associated with distinct absorptions and reveals the presence of multiple ultragap states.

The 182- and 174-cm^{-1} peaks are observed in the RR data from chloride-contaminated PtBr samples. In such samples, peaks at 181 and 210 cm^{-1} maintain constant relative intensities and appear to provide a measure of the level of contamination.[2(b)] These two peaks dominate the RR data acquired with excitations above the IVCT edge.[5(g)] The decreased intensity for the 182- and 174-cm^{-1} peaks in the chloride-free samples indicates that these ultragap states are valence defects for the PtBr chain that are stabilized by the presence of chloride. Such defects may be attracted to the boundary regions between PtCl and PtBr domains and can, therefore, also be associated with edge states. Because the 182- and 210-cm^{-1} peaks maintain constant relative intensities in the mixed-halide samples with greater than 10% chloride doping but not in the more lightly doped PtBr samples, multiple origins of the 182-cm^{-1} peak are suggested.

Figure 8 shows the temperature dependence of the RR data for the ultragap states in PtBr(M). Increased temperature results in substantial loss in the 174-cm^{-1} defect mode intensity. This suggests that the ultragap state associated with this mode is photoinduced and stabilized at lower temperatures but not at room temperature. This is to be contrasted with data acquired for chloride-contaminated samples where the 182- and 210-cm^{-1} peaks remain predominant even at room temperature.[5(g)] Comparison of Figs. 7 (2.41-eV excitation) and 8 reveals sample dependence in the PtBr crystals provided by the present synthetic route. The intensities of the 174- and 182-cm^{-1} peaks relative to the ν_1 mode vary between those two figures, which display Raman data from samples from two different batches of PtBr(M), and these peaks can even vary from crystal to crystal within a single batch. The source of this heterogeneity is not clear, but because the defect modes appear to be photoinduced, these differences may be due to experimental variations apart from sample heterogeneity.

Lattice dynamics

The observation of multiple defect phonons and defect interconversion engenders an attempt to assign these modes. Because the valence defects may be spatially more diffuse in PtBr (see the EPR data, below), any attempt to use classical lattice dynamics in order to derive a reasonable set of force constants for such a disperse defect is contingent on an unacceptable number of assumptions. However, it may be the case that for some defects the lattice is structurally rearranged so that the site becomes localized. We have developed a simple method to

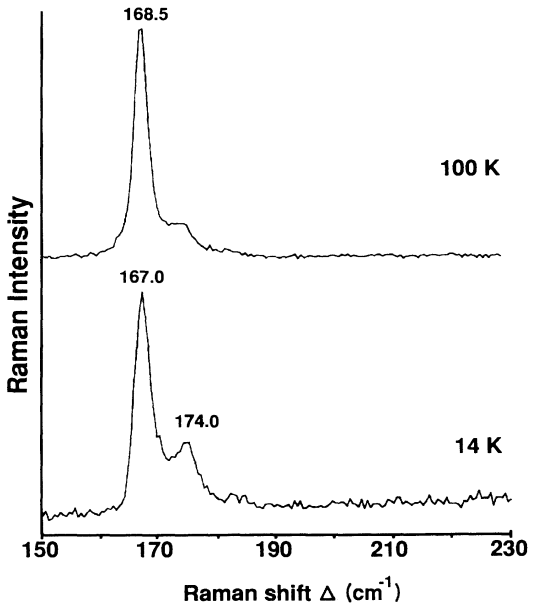

FIG. 8. The temperature dependence of the Raman spectrum of a sample of PtBr(M) obtained with 2.41-eV excitation.

estimate the force constants associated with such defects and have successfully used this technique to characterize defects in PtCl.[12] At the heart of this method is the derivation of the ratio of the force constants associated with the long and short metal-halide bonds. These force constants are referred to as K_2 and K_1, respectively. In PtCl, the K_2/K_1 ratio was determined to be approximately 0.3. By means of similar considerations, this ratio has been estimated to be roughly 0.4 in PtBr. Consideration of various localized defects was included in this exercise, and the expected force field for an electron bipolaron played a key role in the estimation of this ratio. In the most simplified (localized) model, an electron bipolaron may be considered as a series of three consecutive reduced metal sites:

$$\text{Br}\text{--}\text{Pt}^{\text{IV}}\text{--}\text{Br}\text{-----}\text{Pt}^{\text{II}}\text{----}\text{Br}\text{-----}\text{Pt}^{\text{II}}\text{----}\text{Br}\text{-----}\text{Pt}^{\text{II}}\text{----}\text{Br}\text{--}\text{Pt}^{\text{IV}}\text{--}\text{Br}\ .$$

In such a picture, all of the Pt^{II}-Br bonds may be considered to have the force constant of the normal chain reduced metal site-halide bond: K_2. Given this model, several interesting predictions are made. First, with K_2/K_1 equal to 0.37, the primary Raman-active phonon for the electron bipolaron is found at 130 cm^{-1}. The infrared counterpart is then predicted to lie near 140 cm^{-1}. Consistent with this description, the photoinduced 130-cm^{-1} mode does not appear to be associated with a paramagnetic defect, as is seen after analysis of the temperature response of the EPR and Raman signals *(vide infra)*. Nevertheless, this model can be considered to be useful only if such defects are quite localized. Localization of electron bipolarons may occur if the chain becomes kinked in order to accommodate six consecutive long Pt^{II}–Br bonds. This is an interesting possibility that could explain the unusual breadth of the 130-cm^{-1} peak. The multiple environments possible for such a kinked chain site could lead to inhomogeneous broadening of the bipolaron phonon signals, while the attendant symmetry lowering could lead to mixing of the infrared- and Raman-active phonons. As can be seen in Fig. 2, the 130-cm^{-1} peak does not appear to broaden substantially upon warming, which might be expected if the defect increases its size upon warming. However, there is no obvious reason for the chain to prefer localization and distortion in favor of an extended defect configuration. Other localized defects have been explored for PtBr with $K_2/K_1=0.37$ and, among these, the electron polaron is predicted to yield a mode at 150 cm^{-1}. Thus, the intriguing possibility that electron bipolarons are "melting" to form electron polarons (that are subsequently trapped) is raised by the temperature dependence of the Raman data for PtBr(O).

A very interesting alternative to the assignments from the localized classical dynamics has recently been developed by Batistić and Bishop.[13] Using the random-phase approximation in association with the phonon portion of the two-band, three-quarter-filled Hamiltonian, they have generated excitation profiles for the phonons from a number of valence defects. Several consistent results are obtained, including the expectation of extended defects, and, for a hole polaron, the appearance of a broad feature near 130 cm^{-1}, a 150-cm^{-1} sharp peak, and a weak mode at 80 cm^{-1}, the last of which may correspond to the experimentally observed photoinduced 90-cm^{-1} peak. However, the apparent lack of paramagnetic character associated with the 130-cm^{-1} peak in PtBr(M) and the suggestion of distinct origins for the 130- and 150-cm^{-1} signals based on the temperature-dependent relative intensities of these two modes does not appear to support this assignment. In general, however, these calculations provide the possibility of describing the phonons associated with extended defects, and, for weak or intermediate CDW systems, may represent the only practical approach to this problem.

The ν_1 mode

While we have concentrated to this point on the generation and temperature dependence of the photoinduced defects, the effect of temperature variation on the charge-density wave of the unperturbed chain is also of interest. Figure 9 displays the ν_1 peak of a sample of PtBr(M) obtained with 1.26-eV excitation as a function of temperature. The remarkable result from this data is the observation of softening in the ν_1 energy (170–166 cm^{-1}) as the temperature is decreased. Interestingly, the ν_1 mode does not appear to respond in a dramatic fashion to the phase change at 29.8 °C. Phonon softening upon cooling is contrary to the usual increase in phonon energy observed in solids upon cooling as expected due to contraction of the lattice, but can be explained as a result of weakening of the CDW as the temperature is lowered.

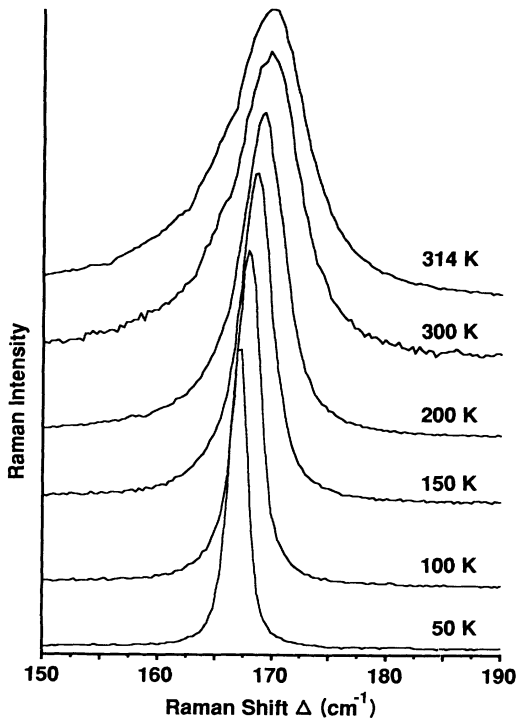

FIG. 9. The temperature dependence of the ν_1 peak of a sample of PtBr(M) obtained with 1.30-eV excitation (no photolysis).

The temperature dependences observed in the x-ray crystallography and the IVCT absorption edge energy are consistent with this explanation. The structural studies reveal that the ratio of the short and long bromide-platinum bond lengths increases as the temperature is reduced.[14] Thus, the Peierls distortion is diminished as the crystals are cooled. Interestingly, some *MX* chains exhibit negative thermal coefficients of expansion along the chain axis.[15] The fact that the strength of the CDW is altered by changing temperature further complicates the kinetic behavior of the defects. An analysis of the temperature dependence of the ν_1 mode of PtCl reveals that this CDW is also weakened by lowering the temperature, but the total shift between room temperature and 15 K is only 2 cm^{-1}, which is proportionately a much smaller effect.[16] Surprisingly, the available absorption data do not appear to be consistent with weakening of the CDW as temperature is lowered. To a first approximation, one would predict that the IVCT edge is red shifted upon lowering the temperature if the charge disproportionation is decreased. However, for the PtBr material in which sulfate dianions replace the perchlorate counterions, a blueshift is observed for the IVCT upon cooling.[4(j)] In addition, the IVCT edge for PtCl, which also reveals softening of the ν_1 mode upon cooling, is known to blueshift as the temperature is lowered.[4(a)]

Electron paramagnetic response data

Like PtCl, 4(g) PtBr exhibits a photoinduced EPR signal both for PtBr(*O*) and PtBr(*M*). An example of the EPR data from a photolyzed crystal of PtBr(*M*) is displayed in Fig. 10. The $g=2.3$ signal is associated with $g_\perp$. In PtBr(*O*), this signal appears to be present prior to any intended photolysis while in PtBr(*M*) the signal is not observed prior to irradiation of the sample with light energy above the IVCT edge. In a fashion similar to the 130-cm^{-1} RR feature, photolysis leads to a large increase in the EPR signal intensity for both samples. By comparison to a sample of known paramagnetic density, the number of paramagnetic sites is estimated to be between one per every 10^4-10^5 platinum atoms. Unlike PtCl,[7(a)] there is no resolved Pt hyperfine structure in the EPR signal from PtBr. This is likely an indication of greater delocalization of the paramagnetic defect on the EPR time scale, a suggestion which is supported by this observation of bromide hyperfine structure.

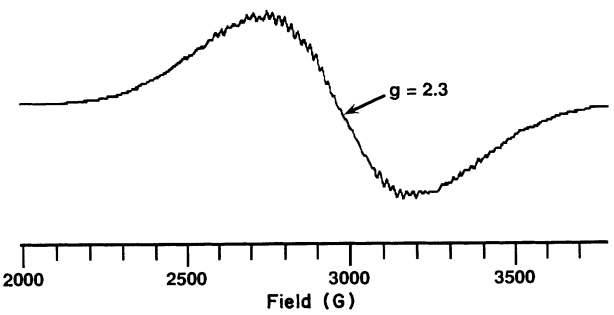

FIG. 10. The EPR spectrum of a photolyzed single crystal of PtBr(*M*). The signal is for $g_\perp$.

We have recently reported a comparison of the EPR spectra in PtCl crystals grown with substitution of ^{15}N in the ethylenediamine ligands with those grown with unsubstituted ligands.[7(c)] Because there is no appreciable change in the hyperfine pattern with 16-G separation, which is superimposed upon the Pt hyperfine structure, we concluded that the 16-G pattern is due to the bridging chloride, rather than to the off-axis nitrogens as has been previously concluded. Until now, no resolved hyperfine structure has been reported for the EPR signal from photolyzed PtBr. However, as can be seen in Fig. 10, this structure can be resolved in some crystals. The number of lines suggests that the spin is delocalized over roughly 7–10 Br sites, which implies a length of chain including 7–10 Pt sites. This should be compared to the EPR signal for PtCl, which reveals Pt hyperfine from two equivalent sites.

Initially, we attempted to measure the loss of EPR signal as a function of time at a given temperature in order to determine the order of the process and the activation energy. However, this approach did not come to fruition because there was no clear alteration of signal intensity at a given temperature and because the EPR signal intensity is nearly completely attenuated at temperatures above 25 K. However, we were able to examine the kinetics of the paramagnetic signal decay by raising the temperature of the helium-transfer cryostat to a desired point and immediately recooling to 10 K for data acquisition. The results of this experiment for a sample of PtBr(*M*) are displayed in Fig. 11. The signal intensity (proportioned to the photoinduced intensity prior to any warming) is seen to decrease to a roughly constant level immediately

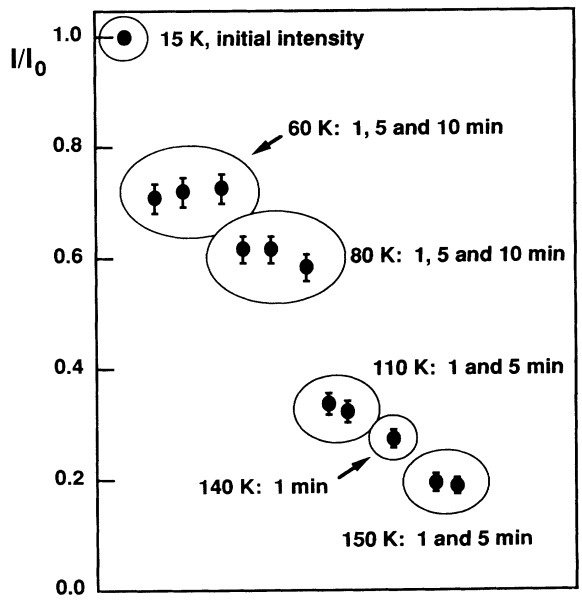

FIG. 11. A comparison of the integrated EPR signal intensity obtained at 10 K for a crystal of PtBr(*M*) after warming to the indicated temperatures for the indicated lengths of time and recooling. The intensities (*I*) are ratioed to the initial photogenerated signal (I_0).

upon warming. Longer times at a given temperature do not result in further significant signal loss; however, warming to a higher temperature does cause a further reduction in the paramagnetic signal. As will be discussed presently, this behavior is consistent with the presence of a range of pinning potentials. Thus, upon warming, the more weakly pinned paramagnetic defects are "shaken loose," while the more deeply pinned defects require more heating to become mobilized. Essentially all of the photoinduced signal in samples of PtBr(M) is lost upon warming to 200 K.

Comparison of the kinetics of the photoinduced RR and EPR signals is worthwhile. Although there are some consistent traits in the generation and temperature dependence of the two types of signals, the fact that we observed loss of approximately half of the intensity of the photoinduced RR peak at 130 cm^{-1} upon warming to 200 K and recooling (not shown) as opposed to complete loss of the EPR signal indicates that these spectral signals derive from distinct types of defects. In support of this, the recovery of the 130-cm^{-1} Raman defect signal upon recooling is distinct from the permanent signal loss observed in the EPR spectrum upon warming to 60 K (cf. Figs. 2 and 11). Comparison of the EPR and Raman results may be complicated by the time-domain differences in these techniques and the time scale of defect mobility.

As noted above, the unusual kinetic behavior observed for decay of the EPR signal points to the existence of variable pinning potentials for the paramagnetic defect or some species that reacts with the paramagnetic defect. These kinetics were modeled using a variable, stepped set of pinning potentials or well depths for the trapped paramagnetic defect. The model includes a selected number of sets of trapping sites, usually 16, with differing pinning potentials and a variable initial population for each set. The rate of decay is assumed to be first order with a rate constant, k_i, given by $k_i = Ae^{E_i/kT}$. The frequency factor A was the same for all sites, usually 1×10^{12} s^{-1}. The pinning potentials E_i were varied in different ways to test the model. The most straightforward variation was to increase the value of E_i by a constant amount, for example, 400 cm^{-1}, beginning with a selected value for E_1. Most of the calculations assumed an equal population of sites for all pinning potentials, but this initial population was also varied in testing the model. The total population of all sites was plotted as a function of time for different temperatures and choices of parameters for well depth, frequency factor, and initial population.

The qualitative features of this model agree well with the observed decay of the EPR signal. Figure 12 illustrates the general nature of the kinetic behavior of such a system. In every case, the signal exhibits rapid decay of some of the defects at a given temperature, followed by a slow loss of defects from the remaining sites of lowest pinning potential. The defects in the deeper wells show no loss over a reasonable time period. The calculated slow loss of paramagnetic defects over a period of several minutes falls within the range of experimental error in our measurement of EPR signal intensity, so that we cannot measure the decay rate with sufficient accuracy to establish the order of the kinetics. The rapid decay over the first few seconds at a given temperature is also not accessible to our measurements.

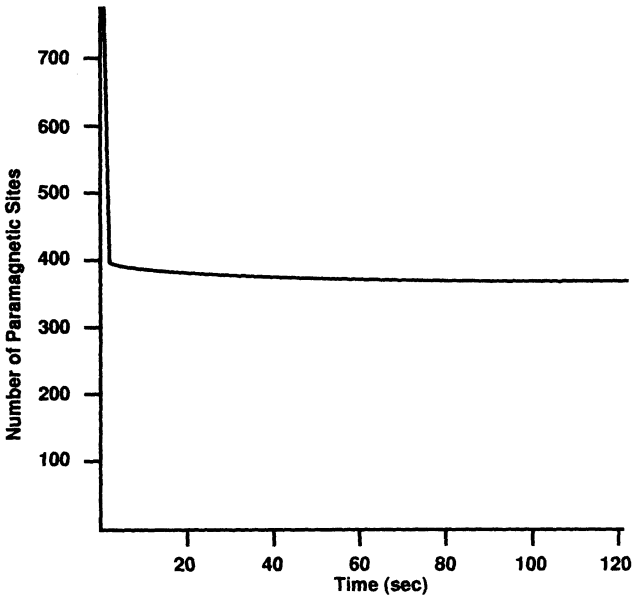

FIG. 12. The predicted effect of warming on the number of paramagnetic sites in an MX chain in which the paramagnetic defects are pinned by a stepped series of potentials.

While exact values cannot be established for the pinning potentials, the modeling results indicate that the well depths must be in the range of a few hundred to a few thousand cm^{-1}. Several possibilities exist for variable potential trapping sites. Likely trapping sites are chain ends, trace impurities, and chain-disorder features. Varying proximity to such features could correspond to differing values of the pinning potential. The steplike nature of the decay of the EPR signal indicates that a range of sites is populated by the paramagnetic defects. The most reasonable interpretation is that the spin defects (or their annihilators) are trapped by the closest pinning site to the exciton formed on absorption of a photon. The EPR signal intensity exhibits saturation upon photolysis with the signal reaching an almost constant level after approximately 1 h. This constant level of spin density suggests a limited number of trapping sites for the paramagnetic defect.

The results presented here do not help to identify the nature of the paramagnetic defect. The defect must involve a Pt(III) (delocalized along the chain) but could be either an electron or hole polaron or a neutral kink. In one series of experiments a different EPR signal at 2100 G was observed after warming and recooling a sample having a photoinduced EPR signal, but this phenomenon was not observed in other samples. Most of the observations indicate only one type of paramagnetic defect.

CONCLUSIONS

Photoinduced defects in both PtBr(M) and PtBr(O) can be observed by absorption, resonance Raman, and EPR spectroscopies. The temperature dependences of

the photoinduced signals indicates that multiple pinning potentials are present, and especially strong defect traps are observed in PtBr(O). The RR data reveal a photoinduced broad peak at 130 cm^{-1} that does not have an associated EPR signal. Classical lattice dynamics suggest that this mode may be due to electron bipolarons that are localized by chain distortion. In PtBr(O), additional defect modes at 160, 155, and 150 cm^{-1} are observed. All of these modes have unique Raman excitation or temperature dependences, which demonstrates that several midgap absorptions are present. These distinct transitions are not revealed in the absorption data. The mobilization of defects upon warming is observed in the Raman data, and in PtBr(O) some of the defects associated with the 130-cm^{-1} signal appear to be converted into deeply trapped defects that yield a peak at 150 cm^{-1}. Excitation above the IVCT reveals several defects that may be associated with the hole bipolaron or hole polaron ultragap states predicted by Bishop *et al.* The temperature dependence of the normal chain ν_1 mode demonstrates that the CDW phase is weakened by lowering the temperature.

With the present information, our tentative description of the defect states created by photolysis is as follows:

$$\text{N.C.} \overset{h\nu}{\rightleftharpoons} P^+ + P^- \overset{P^-}{\underset{-P^- (\text{or} + P^+)}{\rightleftharpoons}} P^+ + BP^- \overset{\Delta}{\rightleftharpoons} P^+ + 2P^-$$

where N.C. is the normal chain, P^+ is the hole polaron, P^- is the electron polaron, and BP^- is the electron bipolaron. In this scheme, photolysis results in creation of electron and hole polarons. These defects may be the decay products of short-lived transients (excitons, breathers, etc.) that have not yet been investigated by time-resolved methods. (Presumably, these transient defects usually revert to the normal chain either in conjunction with emissive or phonon-scattering processes.) The electron polarons remain mobile until they condense into diamagnetic electron bipolarons that are associated with the 130-cm^{-1} Raman signal. The paramagnetic hole polarons are less mobile, pinned by an "external" potential of varying strength in addition to any self-trapping effect, and are the source of the EPR signal. Warming of the electron bipolarons leads to interconversion to electron polarons (either by melting or combination with the hole polarons) and, in PtBr(O), these polarons find pinning sites that are unique to the orthorhombic material. Further warming eventually leads to annihilation of all defects back to the normal chain, with the exception that some electron and hole polarons are trapped in the orthorhombic material even at room temperature.

While this scheme provides tentative assignments of the photoinduced defect spectroscopic signals in PtBr, it cannot represent the entire process by which defects are created and annihilated. As an example, the persistence of the 130-cm^{-1} Raman signal, when compared with the more rapid decay of the EPR signal, shows that complex relaxation processes occur. If the defects that lead to the two spectroscopic signals were purely photogenerated and were the only photoproducts, then the loss of one signal should parallel the loss of the other. Secondary decay paths are almost certainly present. For example, hole polarons, pinned at 15 K, may prefer to condense into hole bipolarons upon activation. By such means, the EPR signal can decay more rapidly than the Raman signal. Another problem is the lack in samples of PtBr(M) of a Raman signal that is readily associated with the paramagnetic defects. The ultragap excitation resonant peaks (171 and 174 cm^{-1}) observed for this material may be due to either paramagnetic or diamagnetic defects or both, but it is not a simple matter to deconvolute the creation and decay of defects that occurs when using these excitation energies in order to investigate this idea. In samples of PtBr(O), the 150-cm^{-1} peak is assigned to paramagnetic electron polaron defects, although the photogenerated EPR signal does not reproducibly yield two distinct signals for this material. The apparent lack of direct creation of such defects upon photolysis, as observed in the Raman data, is surprising but may be due to the relative probabilities of a mobile electron polaron combining with a second electron polaron versus being trapped by one of the unique pinning sites found in the PtBr(O) solid. In samples of PtBr(M), the excitation energies required to achieve resonance with the midgap transitions associated with the hole polarons may lie completely in the 1.0–1.26-eV range, where defect absorption that is not accessible to our current Raman instrumentation is observed. Alternatively, the lack of a Raman signature that can be unequivocally attributed to the hole polaron may be a result of the delocalized nature of the defect (as evidenced by the EPR fine structure). Thus, the rather gentle alteration of valence in the CDW that can be envisioned for such a disperse defect may not yield a Raman-active mode that is readily discernible from the normal chain ν_1 mode.

Perhaps the most significant conclusion to be derived from this study is that the strength of the CDW phase in PtBr is such that the defects are much more delocalized than in the strong CDW solid, PtCl. The strength of the CDW in PtBr can probably best be compared to those in PtCl and PtI by means of examination of the IVCT edge energies. Thus, the occurrence of the edge near 1.5 eV in PtBr, 2.5 eV in PtCl, and 1.0 eV in PtI suggests that the CDW in PtBr is quite weak, and is closer in strength to the charge disproportionation within the PtI solid than to that in PtCl. Accordingly, activation of defects in PtBr is observed at low temperatures in both the Raman and EPR data. However, the kinetic behavior of these defects is dependent upon a number of complicated interactions, including the nature of the original crystalline phase, the presence of variable-strength pinning sites, interconversion of defect states, and the temperature dependence of the strength of the CDW itself. In order to obtain further insight into the effects of the strength of the CDW on the ground and defect properties of MX chains, we intend to pursue similar spectroscopic characterizations of a variety of these intriguing low-dimensional solids, including the Pd analogues of the PtX chains, the PtX chains with different counterions, and, with the acquisition of sensitive infrared detectors, the weak CDW material PtI and the NiBr SDW phase material.

ACKNOWLEDGMENTS

We are very grateful to L. DeGiorgi and M. Haruki for making their results available to us prior to publication. We also acknowledge many useful discussions with Professor Susumu Kurita of Yokohama National University and with Alan Bishop, Ivo Batistic, and Avadh Saxena at the Condensed Matter and Statistical Physics group, T-11, at Los Alamos National Laboratory. Financial support was provided by the Office of Basic Energy Sciences and the Center for Materials Science at Los Alamos National Laboratory.

---

*To whom correspondence should be addressed.

†Permanent address: Department of Chemistry, Furman University, Greenville, SC 29613.

‡Permanent address: Laboratoire de Physique de l'Etat Condensé, Faculté des Sciences, Universite du Maine, 72017 Le Mans CEDEX, France.

[1]For a general review, see J. S. Miller and A. J. Epstein, Prog. Inorg. Chem. **20**, 1 (1976).

[2]Synthesis: (a) F. Basolo, J. C. Bailar, Jr., and B. R. Tarr, J. Am. Chem. Soc. **72**, 2433 (1950); (b) S. C. Huckett, R. J. Donohoe, L. A. Worl, A. D. F. Bulou, C. J. Burns, J. R. Laia, D. Carroll, and B. I. Swanson, Chem. Mater. **3**, 123 (1991).

[3]Theory: (a) K. Nasu, J. Phys. Soc. Jpn. **52**, 3865 (1983); (b) K. Nasu and A. Mishima, Rev. Solid State Sci. **2**, 539 (1988); (c) D. Baeriswyl and A. R. Bishop, J. Phys. C **21**, 339 (1988); (d) A. Mishima and K. Nasu, Phys. Rev. B **39**, 5758 (1989); (e) S. D. Conradson, M. A. Stroud, M. H. Zietlow, B. I. Swanson, D. Baeriswyl, and A. R. Bishop, Solid State Commun. **65**, 723 (1988); (f) A. Mishima and K. Nasu, Phys. Rev. B **39**, 5763 (1989); (g) A. R. Bishop, J. T. Gammel, and S. R. Phillpot, Synth. Met. **29**, F151 (1989); (h) J. T. Gammel, R. J. Donohoe, A. R. Bishop, and B. I. Swanson, Phys. Rev. B **42**, 10 566 (1991); (i) A. R. Bishop, Synth. Met. (to be published).

[4]Electronic spectroscopy: (a) M. Tanaka, S. Kurita, T. Kojima, and Y. Yamada, Chem. Phys. **91**, 257 (1984); (b) N. Matsushita, N. Kojima, T. Ban, and I. Tsujikawa, J. Phys. Soc. Jpn. **56**, 3808 (1987); (c) N. Kuroda, M. Sakai, Y. Nishina, M. Tanaka, and S. Kurita, Phys. Rev. Lett. **58**, 2122 (1987); (d) M. Tanaka, S. Kurita, M. Haruki, and M. Fujisawa, Synth. Met. **21**, 103 (1987); (e) S. Kurita, M. Haruki, and K. J. Miyagawa, J. Phys. Soc. Jpn. **57**, 1789 (1988); (f) M. Haruki and S. Kurita, Phys. Rev. B **39**, 5706 (1988); (g) S. Kurita and M. Haruki, Synth. Met. **29**, F129 (1989); (h) N. Matsushita, N. Kojima, N. Watanabe, T. Ban, Solid State Commun. **71**, 253 (1989); (i) N. Matsushita, N. Kojima, T. Ban, and I. Tsujikawa, Bull. Chem. Soc. Jpn. **62**, 1785 (1989); (j) **62**, 3906 (1989); (k) R. J. Donohoe, S. A. Ekberg, C. D. Tait, and B. I. Swanson, Solid State Commun. **71**, 49 (1989).

[5]Raman spectroscopy: (a) G. C. Papavassiliou and T. Theophanides, J. Raman. Spectrosc. **7**, 230 (1978); (b) G. C. Papavassiliou, T. Theophanides, and R. J. Rapsomanikis, *ibid.* **8**, 227 (1979); (c) G. C. Papavassiliou and T. Theophanides, Z. Naturforsch. Teil B **34**, 986 (1979); (d) R. J. H. Clark and M. J. Kurmoo, J. Chem. Soc. Faraday Trans. **79**, 519 (1983); (e) R. J. H. Clark, in *Advances in Infrared and Raman Spectroscopy*, edited by R. J. H. Clark and R. E. Hester (Wiley Heyden, New York, 1984), Vol. 11, p. 95, and references therein; (f) M. Tanaka and S. Kurita, J. Phys. C **19**, 3019 (1986); (g) S. D. Conradson, R. F. Dallinger, B. I. Swanson, R. J. H. Clark, and V. B. Croud, Chem. Phys. Lett. **135**, 463 (1987); (h) R. J. Donohoe, R. B. Dyer, and B. I. Swanson, Solid State Commun. **73**, 521 (1990); (j) B. I. Swanson, Synth. Met. (to be published).

[6]Infrared spectroscopy: (a) L. DeGiorgi, P. Wachter, M. Haruki, and S. Kurita, Phys. Rev. B **40**, 3285 (1989); (b) *ibid.* **42**, 4341 (1990).

[7]Electron paramagnetic resonance: (a) A. Kawamori, R. Aoki, and M. Yamashita, J. Phys. C **18**, 5487 (1985); (b) N. Kuroda, M. Sakai, M. Suezawa, Y. Nishina, and K. Sumino, J. Phys. Soc. Jpn. **59**, 3049 (1990); (c) C. A. Arrington, C. J. Unkefer, R. J. Donohoe, S. C. Huckett, S. Kurita, and B. I. Swanson (unpublished).

[8]Crystallography: (a) N. Matsumoto, M. Yamashita, I. Ueda, and S. Kida, Mem. Fac. Sci. Kyushu Univ. Ser. C **11**, 209 (1978); (b) H. J. Keller, R. Martin, and U. Traeger, Z. Naturforsch. **33B**, 1263 (1978); (c) N. Matsumoto, M. Yamashita, S. Kida, and I. Ueda, Acta Crystallogr. Sect. B **35**, 1458 (1979); (d) H. Endres, H. J. Keller, R. Martin, H. N. Gung, and U. Traeger, *ibid.* **35**, 1885 (1979); (e) H. Endres, H. J. Keller, R. Martin, U. Traeger, and M. Novotny, *ibid.* **35**, 35 (1980); (f) H. J. Keller, B. Müller, G. Ledezma, and R. Martin, Acta Crystallogr. Sect. C **41**, 16 (1985); (g) M. Yamashita, K. Toriumi, and T. Ito, *ibid.* **41**, 876 (1985).

[9]K. Toriumi, Y. Wada, T. Mitani, S. Bandow, M. Yamashita, and Y. Fujii, J. Am. Chem. Soc. **111**, 2341 (1989).

[10]A. Saxena, J. T. Gammel, and A. R. Bishop (unpublished).

[11]M. Haruki and P. Wachter, Physica B (to be published).

[12](a) A. D. F. Bulou, R. J. Donohoe, and B. I. Swanson, J. Phys. C (to be published); (b) C. E. Paraskevaidis, C. Papatriantafillou, and G. C. Papavassiliou, Chem. Phys. **37**, 389 (1979).

[13]I. Batistić and A. R. Bishop, Phys. Rev. B **45**, 5282 (1992).

[14]S. C. Huckett, C. J. Burns, E. Garcia, T. Franckom, and B. I. Swanson (unpublished).

[15]M. Tanaka, I. Tsujikawa, K. Toriumi, and T. Ito, Acta Crystallogr. Sect. B **38**, 2793 (1982).

[16]R. J. Donohoe (unpublished data).